39th IAHR WORLD CONGRESS GRANADA, SPAIN 2022 From Snow to Sea 19-24 June 2022

Proceedings of the 39th IAHR World Congress
19–24 June 2022, Granada, Spain
doi://10.3850/IAHR-39WC2521716X2022504

Do Antidune Trains Undergo Morphological Changes When These Bedforms Migrate Upstream?

Ivan Pascal [1], Patricio Bohorquez [2] and Christophe Ancey [3]

[1,3] Laboratoire Hydraulique Environnementale, École Polytechnique Fédérale de Lausanne, Lausanne, Switzerland
ivan.pascal@epfl.ch, christophe.ancey@epfl.ch

[2] Centre of Advanced Studies in Earth Science, University of Jaen, Jaen, Spain
patricio.bohorquez@ujaen.es

Abstract

Upstream migrating antidunes develop in streams under supercritical flow conditions. These bedforms are often organised in trains (i.e. sequences of well-developed antidunes). In shallow flows over coarse sediments, the dynamics of a single antidune can be significantly influenced by the surrounding bedforms. The drivers and behaviour of these interactions remain unclear. We conducted an experimental study to investigate the morphodynamics of antidune trains in narrow streams with a particular focus on mechanisms that could systematically influence bedform geometry as antidunes migrate upstream. The incipient antidunes near the flume outlet (which is a bed discontinuity) often exhibited migration periods notably longer than the typical value observed further upstream. Far from the boundaries, antidune sequences were mostly affected by transient downstream travelling disturbances and we did not observe any systematic change of antidune shape and dynamics along their migration path. Such insights into potential sources of non-uniformity are helpful for interpreting the differences between the outcomes of experimental and numerical simulations.

Keywords: Antidune; Mountain stream; Bedload transport; Non-uniform flow; Gravel-bed river.

1. INTRODUCTION

Antidunes are bedforms for which the flow free surface is nearly in phase with the bed undulation (Kennedy, 1961). These bedforms develop in supercritical or near-critical flows and migrate upstream, downstream or remain approximately stationary (Núñez-González and Martín-Vide, 2011; Kennedy, 1961). Antidunes may be two-dimensional (also called 'long-crested') or three-dimensional ('short-crested') depending on flow, sediment and boundary conditions (Kennedy, 1961). They often form sequences of bedforms called trains. Multiple sequences of downstream migrating 3D antidunes have been observed to coexist with alternate bars in flume experiments (Inoue et al. 2020). Upstream migrating antidunes (see Fig. 1) are the most documented ones in both experimental and field studies.

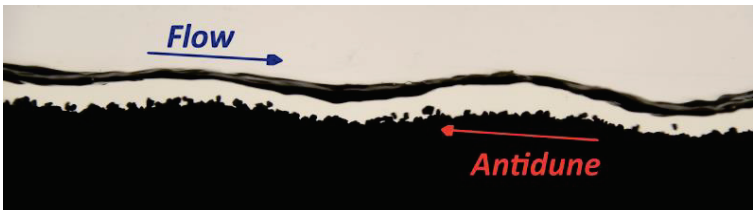

Figure 1. Upstream migrating antidunes similar to those observed during ES1. Flow depth $h \approx 1$ cm.

As stated by Recking et al. (2009), antidunes may develop in steep streams also at moderate flow rates once the effective shear stress on bed particles exceeds the critical threshold for incipient sediment transport. In these streams, antidunes have been identified as one of the mechanisms that may lead to the formation of step-pool sequences (Chin, 1999; Grant, 1994; Whittaker and Jaeggi, 1982). During experimental runs conducted for supercritical flows over steep slopes made of uniform gravel, Mettra (2014) observed upstream migrating antidunes characterised by variable wave geometry and celerity. In a recent study (Pascal et al., 2021), this variability was specifically investigated by running steady-state experiments in a narrow 2.5-m-long flume with nearly constant bed slope angle ($\psi \approx 3°$) and four different levels of bedload transport intensity. Long-crested antidunes developed and migrated upstream during those experimental runs. The bed topography profile was monitored in a control window over time and the celerity vs. wavelength (c-λ) spectra were computed by applying 2D fast Fourier transform (2D-FFT) on the bed elevation perturbation data. The c-

λ spectra for upstream migrating antidunes followed positive trends (i.e. the longest antidunes typically migrated faster than the shortest ones), oppositely to those found for dunes with analogous 2D spectral representations (see Guala et al. 2014). Particular downstream travelling perturbations which locally disrupted the antidune sequences were also identified (see Fig. 11 in Pascal et al., 2021).

Cyclic occurrence and breaking of trains composed by antidunes with variable geometry have been documented in natural rivers (e.g. see Movie S2 in Froude et al., 2017). Cartigny et al. (2014) reported trains of antidunes which evolved in cyclic steps as they migrated upstream during experiments carried out with fine sand and at high sediment transport rates. Bohorquez and Ancey (2016) simulated numerically a supercritical flow over fine gravel in an 8-cm-wide 1.5-m-long flume. Their simulation produced antidunes that grew significantly in both wavelength and amplitude during their upstream migration. This phenomenon was not identified during the experiments performed by Mettra (2014) and Pascal et al. (2021), both using short and narrow flumes, thus the question remains open: Do systematic morphological changes occur in the antidunes during their upstream migration within trains? We conducted a new experimental campaign in a longer flume to assess the potential appearance of these changes. Such bedform evolution might increase flow non-uniformity – which is already an innate feature of flows over antidunes – in steep streams under supercritical flow regime and low to moderate bedload transport intensity. In this paper, we outline results of an experiment characterised by conditions similar to the E1 run of Pascal et al. (2021) but conducted in a 5.8-m-long flume. The bed elevation profile was monitored by using lateral cameras and image-based detection of the bed-water interface. Continuous wavelet transform (CWT) analysis was conducted in addition to the previously mentioned 2D-FFT analysis. We investigated antidune morphodynamics within antidune sequences in the upstream sector of the flume as well as close to the flume outlet. This study also provided useful information regarding the interactions of antidunes with artificial structures which interrupt the bed continuity in steep mountain rivers.

2. METHODS

2.1 Experimental Setup and Conditions

The experiment (ES1) was carried out in a 4-cm-wide flume with active length L_f = 5.8 m. ES1 was conducted under steady-state conditions with active sediment feeding at the flume inlet and lasted 60 minutes. We used well-sorted dark gravel characterised by median particle diameter d_{50} = 2.5 mm, mean particle volume $V_p = 8.5 \cdot 10^{-8}$ m^3 and sediment density ρ_s = 2550 kg m^{-3}. We imposed the sediment feeding rate $q_{s,in}$ and the mean bed slope angle $\psi_{av,ES1}$, and we adjusted the water discharge to a constant value that maintained the balance between erosion and deposition at the flume scale (i.e. near-constant overall mean bed slope over time). At the flume outlet, a 15-cm-long 4-cm-high plastic box filled with gravel (with perforated vertical walls and smooth top face) acted as a permeable weir. We refer to its upstream perforated wall as the 'septum'. The values of the main experimental parameters measured or estimated during ES1 are summarised in Table 1. The flow regime was turbulent and markedly supercritical.

Table 1. Main experimental parameters for the run ES1.

	$\psi_{av,ES1}$ [°]	$q_{s,in}$ [m^2 s^{-1}]	$q_{s,av\text{-}ES1}$ [m^2 s^{-1}]	q_w [m^2 s^{-1}]	R_b (h_0) [mm]	Fr [-]	Re [-]	Θ [-]	Θ_c [-]
ES1	2.7	$1.79 \cdot 10^{-5}$	$1.77 \cdot 10^{-5}$	$4.4 \cdot 10^{-3}$	9 (10)	1.4	4400	0.107	0.065

The Shields parameter Θ was estimated as

$$\Theta = \frac{R_b \tan \psi_{av}}{d_{50}\,(s-1)}, \qquad [1]$$

where g is the gravitational acceleration, ρ is the water density, $s = \rho_s / \rho$ is the sediment-to-water density ratio and R_b is the bed hydraulic radius. We used the Einstein-Johnson correction method (Einstein, 1942; Johnson, 1942) to compute R_b based on the reference flow depth h_0, analogously to the framework adopted in our previous work (see Pascal et al., 2021). Note that $h_0 \simeq h_{Dav}$, where h_{Dav} is the time-space averaged depth and h_0 is the reference flow depth calculated with a Colebrook-type relationship for rough fully-turbulent flows. The mean critical Shields value Θ_c for ES1 was estimated according to Recking et al. (2008) as

$$\Theta_c = 0.15(\tan \psi_{av})^{0.275}. \qquad [2]$$

2.2 Bed topography and bedload transport monitoring systems

For the bed topography monitoring, we used two control windows (identified as TCW1 and TCW2). This choice was made to ensure highly accurate topography profiles. Each control window was filmed from the side by an acA4112-30um Basler camera (operated at 1 fps) equipped with a Computar 1:2.8 f = 25 mm C-mount 1.1" lens. TCW1 covered the sector from x = 0.66 m to x = 2.18 m (x = 0 m indicated the upstream edge of the granular bed), whereas TCW2 covered the sector from x = 4.06 m to x = 5.80 m (the last coordinate corresponded to the downstream edge of the granular bed and to the outlet septum). The nominal image resolution factor was approximately 0.43 mm/px for both control windows. On the side of the flume opposite to the cameras a series of backlight panels ensured a uniform bright background. Therefore, applying a binarization filter on the raw image allowed us to detect the approximate contour of the bed profile. Since antidunes in this experiment were nearly two-dimensional, monitoring the bed topography profile was sufficient to measure antidune wavelength and amplitude. Images were affected by lens distortion and by the opposite perspective distortion effect, and so was the wavelength measurement. The errors due to distortions impacted particularly the topography profiles near the edges of the control windows. We indirectly estimated a maximum error at about 3 d_{50} for the wavelength values. The final dataset collected for each control window j was a $Z_{0,TCWj}$ (x,t) matrix of the bed elevation z values corresponding to the sampling points with {x,t} coordinates.

During ES1 we continuously monitored the bedload transport rates at the flume outlet. The monitoring was based on particle tracking applied to the image sequences collected by using an acA2000-165um Basler high-speed camera (lens: Fujinon TV 1:1.7 / 35 mm, f/5.6). The particles were filmed while they were passing over a white board right downstream of the outlet septum. The camera was operated at 100 frames per second. The tracking routine was very similar to that adopted by Ancey and Pascal (2020). We used an adapted version of the TrackMate plugin (Tinevez et al., 2017) from the ImageJ platform (Schindelin et al., 2015) in which we modified the linking cost function of the LAP tracker (Jaqaman et al., 2008) to account for the dominant particle motion imposed by the unidirectional flow (in downstream direction) over the outlet plate. The bedload transport flux was calculated as volume-averaged rate (Ancey et al., 2008) using the expression

$$q_s(t) = \frac{V_p\, N(t)}{W\, L} U_p(t), \qquad [3]$$

where W is the flume width, L= 4 cm is the control volume length in streamwise direction, U_p (t) is the averaged streamwise velocity of the particles present at time t in the control window and N (t) is the number of moving particles. We calculated time-volume averages $q_{s,av}$ ($t \mid \Delta t$) for Δt-wide intervals centred at time t. The parameter $q_{s,av\text{-}ES1}$ (in Table 1) refers to the run-averaged rate $q_{s,av}$ (t = 1800 s $\mid \Delta t$ = 3600 s).

2.3 Bed topography analysis

The framework for topography analysis started with three preliminary steps. First, we selected the submatrix of interest $Z_{0,TCWj}$([x_a x_b], [t_a t_b]) within a bed elevation matrix $Z_{0,TCW\,j}$ (x,t). Second, we calculated the bed slope time series, and we assessed its stationarity to identify possible signs of marked deviations from the steady-state condition. As third step, we computed the bed elevation perturbation matrix Z_{TCWj} ([x_a x_b], [t_a t_b]) by subtracting its linear trend from each row in the matrix $Z_{0,TCWj}$ ([x_a x_b], [t_a t_b]).

Spectral analysis was conducted to assess possible systematic changes in the antidune morphodynamics over the flume length. To that end, we selected the entire bed elevation perturbation matrices, Z_{TCW1} ([x_a = 0.66 m x_b = 2.18 m], [t_a = 0 s t_b = 3600 s]) and Z_{TCW2} ([x_a = 4.06 m x_b = 5.80 m], [t_a = 0 s t_b = 3600 s]). We then applied a 2D-FFT in temporal and spatial frequency domain to each matrix. Subsequently, we computed the power spectral density that corresponded to each {λ,T} pair (where T indicates the wave period) by using the Fourier coefficients which resulted from the 2D-FFT. Finally, the T-λ spectra could be converted in c-λ spectra by considering the relationship

$$c = \frac{\lambda}{T}. \qquad [4]$$

The spatial and temporal variabilities in the morphodynamics of the antidune pattern were also investigated by applying continuous wavelet transform (CWT). Wavelet analyses have been extensively used in geophysics during the last decades, and in the characterization of bed morphologies (e.g. Singh et al., 2011; Cataño-Lopera et al., 2009; Little et al., 1993). Applying wavelet transform to a time series allows to efficiently estimate its "dominant modes of variability and how these modes vary in time" (Torrence and Compo, 1998). We chose the Morlet function as mother wavelet. The 'wt' function included in the 'wavelength-coherence' MATLAB package (Grinsted et al., 2004) was used for the CWT application. We performed signal analyses in space domain (longitudinal bed profiles $Z_t(x)$ collected at subsequent times) and in time domain (time series of the bed elevation perturbation $Z_x(t)$ at given cross-sections x_{fixed}). We mainly focused on the

Z_{TCW2} data because we were interested in investigating possible local non-uniformities that occurred in the antidune trains near the flume outlet. For the results presented in this paper, we computed and analysed CWT power scalograms and 1D spectra. We considered the 'cone of influence' (which identifies the zones of the scalogram in which the edge artefacts are non-negligible) as formulated by Grinsted et al. (2004). The power peaks in the scalograms were compared to a background red noise spectrum—as defined by Grinsted et al. (2004) according to Torrence and Compo (1998)—to assess their statistical significance.

3. RESULTS

3.1 Antidune patterns during ES1

During ES1, long-crested antidunes formed and migrated upstream (Fig. 2 and Fig. 3). The bedform sequences were affected by downstream travelling disturbances. Their overall behaviour in the two control windows was similar to that observed during previous experiments in a shorter flume (see run E1 in Pascal et al., 2021).

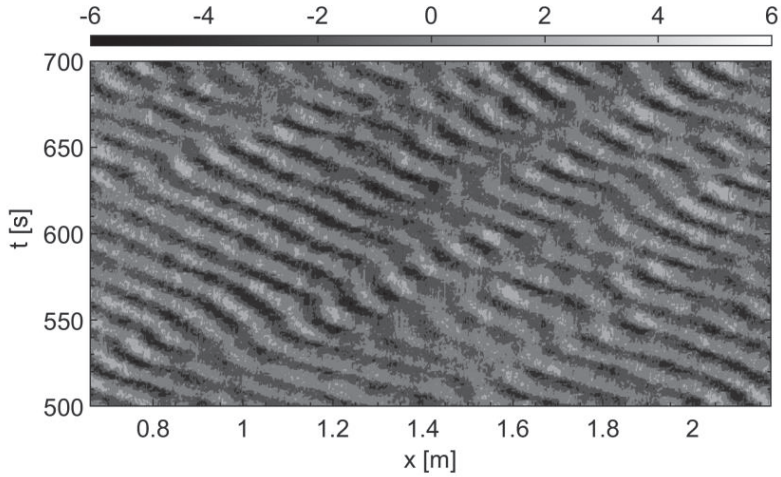

Figure 2. Contour plot of the bed elevation perturbation Z_{TCW1} from t = 500 s to t = 700 s. Colorbar units correspond to [mm].

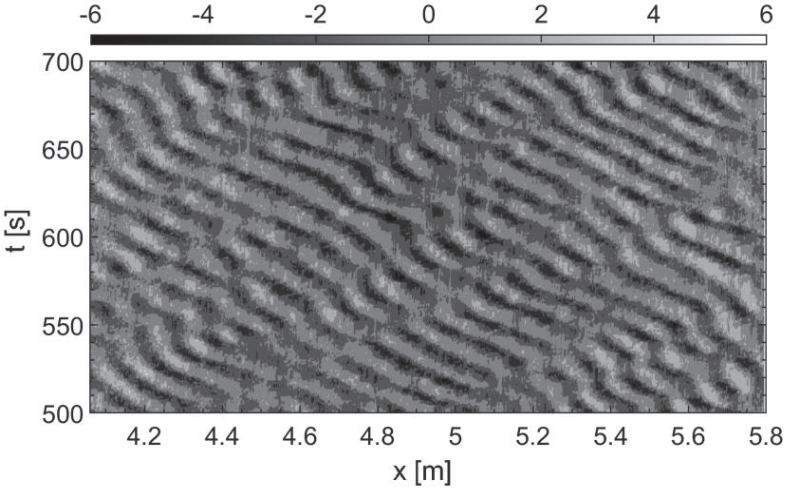

Figure 3. Contour plot of the bed elevation perturbation Z_{TCW2} from t = 500 s to t = 700 s. Colorbar units correspond to [mm].

3.2 Celerity-wavelength spectra

As one can see in Fig. 4, the c-λ spectra computed for Z_{TCW1} and Z_{TCW2} were very similar. Their common trends suggest that the typical antidune dynamics did not vary between the two regions. The wavelength also fell within the same range of values. In agreement with the findings by Pascal et al. (2021), antidune trains were composed of bedforms whose wavelength λ varied in the 0.6–2 λ_{R09} range (see Fig. 4 and Fig. 6), where λ_{R09} = 13 cm is the expected dominant wavelength estimated by using the relationship proposed by Recking et

al. (2009) (with the parameters reported in § 2.1). Therefore, under the ES1 experimental conditions, the antidune sequences did not manifest any systematic increase in their wavelength during the upstream migration from TCW2 towards TCW1. This contradicts the results of the numerical simulation ran by Bohorquez and Ancey (2016). It is worth mentioning that the conditions imposed in their numerical simulation led to a mean bedload transport rate $q_{s,av\text{-}B16} = 6\, q_{s,av\text{-}ES1}$, which corresponded to a dimensionless Einstein rate $\Phi_{av\text{-}B16} = 1.7\, \Phi_{av\text{-}ES1}$ and to a mean total particle flux around 86 part. s^{-1} (84 part. s^{-1} for ES1). The outcomes of ES1 suggest that if any 'nonlinear coarsening' mechanism (hypothesised by Bohorquez and Ancey, 2016) affected the antidune sequences during the run, its effects on the bedform shape were damped by some opposite process (perhaps associated with the downstream travelling disturbances).

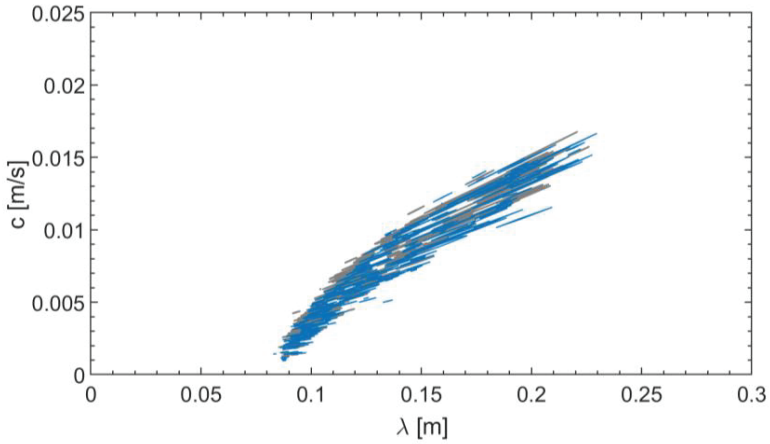

Figure 4. Contours of the c-λ spectra for Z_{TCW1} (grey) and Z_{TCW2} (blue). Contour lines are set for the same normalised density level.

3.3 Non-uniformity: description and quantification by wavelet analyses

The previous section showed that no systematic morphological change of the antidunes occurred during their upstream migration along the central part of the flume. Signs of transient and localised non-uniformities in the antidune trains were evident from the visual inspection of the bed elevation perturbation plots (Fig. 2 and Fig. 3). The antidune sequences appeared particularly prone to non-uniformities in shape and celerity in the close vicinity of the flume outlet (i.e. between $x \approx 5.5$ m and $x = 5.8$ m, Fig. 3). The analyses based on CWT allowed us to confirm this impression and to conduct a quantification of the "irregularities" localised near the flume outlet. Figure 5 shows the 1D wavelet period spectra computed from the time series of the bed elevation perturbation $Z_x(t)$ at different x_{fixed} coordinates.

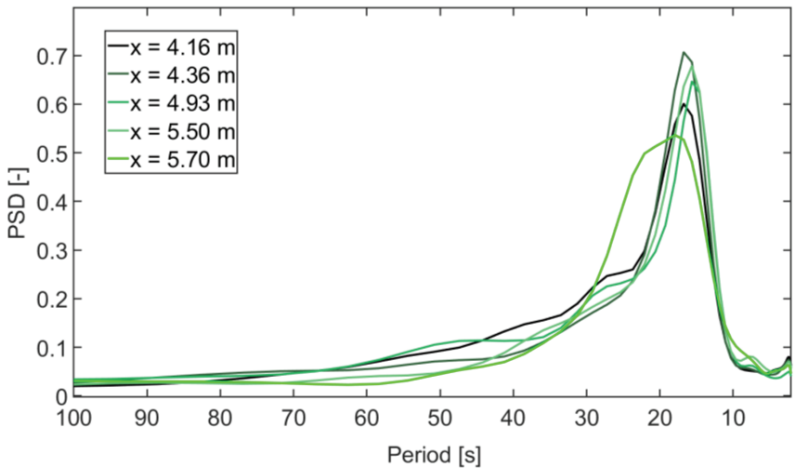

Figure 5. 1D wavelet spectra of the bed elevation perturbation $Z_x(t)$ at different x_{fixed} coordinates in TCW2.

All the spectra in Fig. 5 that were computed from $Z_x(t)$ signals with $x_{fixed} \leq 5.5$ m displayed sharp peaks for period values between 15 s and 20 s. The $Z_{x=\,5.70\ m}(t)$ spectrum was characterised by a wider bell shape

compared to the other spectra. Its power spectral density in the 20–30 s band was particularly high. The shape of this spectrum indicates that close to the flume outlet, the antidunes often experienced migration periods notably longer than the typical value (T≈18 s) measured at cross-sections located upstream. The different dynamics of these bedforms might be explained by considering that the lee-side slope of an incipient antidune in contact with the outlet septum could be less prone to erosion (due to the grain contacts with the fixed structure) than that of antidunes far from the outlet. Therefore, we could suppose that occasionally these bedforms (that we might call 'point-antidunes' in analogy with 'point-bars') remained nearly stationary close to the flume outlet—where their size increased—before detaching from the boundary and starting their 'free' upstream migration. Another factor that might affect the antidune dynamics near the flume outlet is the hyporheic flow configuration. Near the septum, the hyporheic flow could be directed downward, upward, or remain almost horizontal—depending on the specific boundary conditions—and thus it might influence the stability of the grains that compose the bedforms.

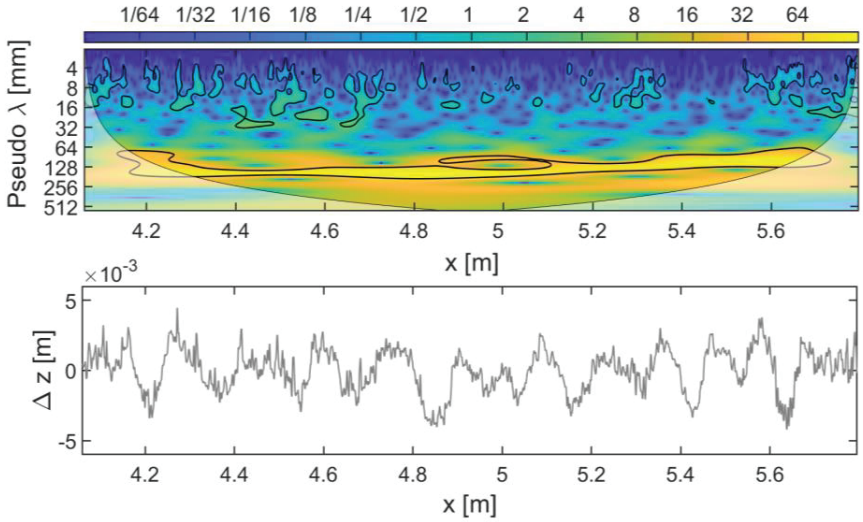

Figure 6. Top: CWT power scalogram for Z_{TCW2} (x, t = 610 s). Black lines indicate the 5% significance contours. Bottom: Z_{TCW2} (x, t = 610 s) plot.

We also applied the CWT to the longitudinal bed profiles collected each second. The resulting time series of CWT power scalograms (see an example in Fig. 6) were useful to visualise in a synthetic manner the wavelength values that characterised the antidune sequences and the transient non-uniformities that affected them. When these disturbances occurred, they propagated downstream before being damped. Occasionally, they marked a migrating discontinuity in the approximately sinusoidal profile of the antidune sequence—that is, a bed patch in which the antidune silhouette was no more discernible for a few seconds (see Fig. 2 and Fig. 3). Pascal et al. (2021) proposed to consider the most persistent discontinuities caused by downstream travelling disturbances as boundaries between different antidune trains (see Fig. 11 in that paper). These discontinuities and the associated antidune splitting (or merging) events typically corresponded to peculiar patterns in the $Z_t(x)$ CWT scalogram. Namely, their x coordinate coincided with scalogram regions characterised by the absence of significant power peaks close to λ_{R09} in the *pseudo-λ* space (or by multiple peaks close to λ_{R09}). These particular patterns in the scalogram identify nearly flat bed or bedforms with complex shape (see the scalogram power and the bed elevation perturbation profile for $x \approx 5$ m in Fig. 6 and the pattern around Z_{TCW2} (x, t = 610 s) in Fig. 3). Usually, when antidunes in a train were characterised by similar (or gently varied) wavelength values they also experienced the most constant migration celerity (compare Fig. 6 and Fig. 3).

4. CONCLUSIONS

Monitoring bed topography on long flume sectors during a steady-state experiment proved fruitful to detect and quantify morphodynamic changes to trains of upstream migrating antidunes. Overall, our experiments in a long flume led to geometry and celerity ranges consistent with the earlier results obtained by Pascal et al. (2021) in a short flume. We did not observe the systematic increase in antidune wavelength shown by the numerical simulation made by Bohorquez and Ancey (2016) for similar conditions.

We found that the bed discontinuity at the flume outlet triggered significant non-uniformities in the antidune morphodynamics. The incipient antidune near the flume outlet septum usually experienced a relatively long phase of growth before starting to migrate upstream with the typical celerity. At given flow discharge and mean bedload transport rate, the influence of the outlet septum on the hyporheic flow conditions likely regulate the magnitude and periodicity of these local non-uniformities. This observation highlights that boundary conditions deserve particular attention when studying bedform dynamics and bedload transport processes even under supercritical flow regime. A few decimeters far from the flume outlet and further upstream, the antidunes trains were mainly affected by transient downstream travelling disturbances whose source remained unknown.

5. ACKNOWLEDGEMENTS

P.B. was funded by “Programa Operativo FEDER 2014-2020” and “Consejería de Economía y Conocimiento de la Junta de Andalucía” under Grant No. 1380967. I.P. thanks Prof. François Gallaire and Prof. Tomás Trewhela for their helpful advices on wavelet transforms at the beginning of his doctoral studies. We are grateful to Bob de Graffenried and Michel Teuscher for their precious assistance in designing and building the new flume. We thank Yannis Bastide and Davide Lamberti for their valuable help during the trial stage of the experimental setup.

6. REFERENCES

Ancey, C., Davison, A.C., Böhm, T., Jodeau, M. and Frey, P. (2008). Entrainment and motion of coarse particles in a shallow water stream down a steep slope. *J. Fluid Mech.*, 595, 83–114.

Ancey, C. and Pascal, I. (2020). Estimating mean bedload transport rates and their uncertainty. *J. Geophys. Res. Earth Surf.,* 125 (7), e2020JF005534.

Bohorquez, P. and Ancey, C. (2016). Particle diffusion in non-equilibrium bedload transport simulations. *Appl. Math. Model.* 40, 7474–7492.

Cartigny, M., Ventra, D., Postma, G. and Den Berg, J.H. (2014). Morphodynamics and sedimentary structures of bedforms under supercritical-flow conditions: New insights from flume experiments. *Sedimentology*, 61, 712–748.

Cataño-Lopera, Y.A., Abad, J.D. and García, M.H. (2009). Characterization of bedform morphology generated under combined flows and currents using wavelet analysis. *Ocean Eng.,* 36(9-10), 617–632.

Chin, A. (1999). On the origin of step-pool sequences in mountain streams. *Geophys. Res. Lett.*, 26(2), 231–234.

Einstein, H. (1942). Formulas for the transportation of bed load. *Trans. Am. Soc. Civil Eng.*, 107, 561–597.

Froude, M.J., Alexander, J., Barclay, J. and Cole, P. (2017). Interpreting flash flood palaeoflow parameters from antidunes and gravel lenses: an example from Montserrat, West Indies. *Sedimentology,* 64, 1817–1845.

Grant, G.E. (1994) Hydraulics and sediment transport dynamics controlling step-pool formation in high gradient streams: a flume experiment. *Dynamics and geomorphology of mountain rivers*. Berlin: Springer, 241–250.

Grinsted, A., Moore, J.C. and Jevrejeva, S. (2004). Application of the cross wavelet transform and wavelet coherence to geophysical time series. *Nonlinear Process. Geophys.*, 11 (5-6), 561–566.

Guala, M., Singh, A., BadHeartBull, N. and Foufoula-Georgiou, E. (2014) Spectral description of migrating bed forms and sediment transport. *J. Geophys. Res. Earth Surf.*, 119, 123–137

Inoue, T., Watanabe, Y., Iwasaki, T. and Otsuka, J. (2020). Three-dimensional antidunes coexisting with alternate bars. *Earth Surf. Process. Landf.*, 45, 2897–2911.

Johnson, J.W. (1942). The importance of side-wall correction in bed-load investigation. *Civ. Eng.*, 12 (6), 329–331.

Kennedy, J.F. (1961). Stationary waves and antidunes in alluvial channels. PhD thesis, California Institute of Technology.

Little, S.A., Carter, P.H. and Smith, D.K. (1993). Wavelet analysis of a bathymetric profile reveals anomalous crust. *Geophys. Res. Lett.*, 20(18), 1915–1918.

Mettra, F. (2014). Morphodynamic mechanisms in steep channels: from local processes to large-scale evolution. Ph.D. thesis, École Polytechnique Fédérale de Lausanne.

Núñez-González, F. and Martín-Vide, J.P. (2011). Analysis of antidune migration direction. *J. Geophys. Res. Earth Surf.* 116, F02004.

Pascal, I., Ancey, C. and Bohorquez, P. (2021). The variability of antidune morphodynamics on steep slopes. *Earth Surf. Process. Landf.*, 46(9), 1750–1765.

Recking, A., Bacchi, V., Naaim, M. and Frey, P. (2009). Antidunes on steep slopes. *J. Geophys. Res. Earth Surf.* 114, F04025.

Recking, A., Frey, P., Paquier, A., Belleudy, P. and Champagne, J. (2008). Feedback between bed load transport and flow resistance in gravel and cobble bed rivers. *Water Resour. Res.*, 44, W05412.

Schindelin, J., Rueden, C.T., Hiner, M.C. and Eliceiri, K.W. (2015). The ImageJ ecosystem: An open platform for biomedical image analysis. *Mol. Reprod. Dev.*, 82 (7-8), 518–529.

Singh, A., Lanzoni, S., Wilcock, P.R. and Foufoula-Georgiou, E. (2011). Multiscale statistical characterization of migrating bed forms in gravel and sand bed rivers. *Water Resour. Res.*, 47(12), W12526.

Tinevez, J.Y., Perry, N., Schindelin, J., Hoopes, G.M., Reynolds, G.D., Laplantine, E., Bednarek, S.Y., Shorte, S.L. and Eliceiri, K.W. (2017). TrackMate: An open and extensible platform for single-particle tracking. *Methods*, 115, 80–90.

Torrence, C. and Compo, G.P. (1998). A practical guide to wavelet analysis. *Bull. Am. Meteorol. Soc.*, 71 (1), 61–78.

Whittaker, J.G. and Jaeggi, M. (1982) Origin of step-pool systems in mountain streams. *J. Hydraul. Div.*, 108(6), 758–773.

